04

Optimization of ion etching processes in micro- and nanoelectronics by influencing on the energy spectrum of ions

© R.R. Khalilullin, V.O. Kuzmenko, A.V. Miakonkikh

NRC „Kurchatov institute“ — Valiev IPT, Moscow, Russia
e-mail: khalilullin@ftian.ru

Received April 28, 2025
Revised July 18, 2025
Accepted July 30, 2025

The possibility of optimization of Atomic Layer Etching through control of the ion energy spectrum in inductively coupled plasma in Argon and its mixtures with Xe was investigated. A hybrid model was developed in COMSOL software using probe diagnostics data. Increasing the bias voltage amplitude linearly raises the average ion energy, while higher oscillation frequency narrows the ion energy distribution function. The addition of Xe reduces silicon etching rates which can be used to increase synergy in the atomic layer etching process. The maximum etching rate is achieved in pure argon plasma; however, the broader ion energy distribution function increases the risk of substrate damage. The results demonstrate the feasibility of tailoring ion energy distribution function to minimize parasitic sputtering in atomic layer etching processes.

Keywords: Atomic layer etching, inductively coupled plasma, ion energy distribution function, RF bias, Ar plasma, Ar/Xe mixture, ion sputtering.

DOI: 10.61011/TP.2026.01.62844.86-25

Introduction

Rapid developments in micro- and nanoelectronics, which are coupled with a continuous reduction in size of integrated circuit components, impose increased demands on the accuracy and reproducibility of nanostructure formation processes. Atomic layer etching (ALE) [1,2] and plasma surface modification [3,4] are among the key technologies enabling the fabrication of micro- and nanometer-scale components. The ALE method, which is based on cyclic alternation of surface modification (in the form of film deposition, chemical processing, or adsorption) and selective removal of the modified layer by ion bombardment, ensures precise material removal with atomic precision. The idealized ALE process has two features: etch rate saturation (the maximum material removal rate, regardless of the duration of the modification and material removal steps) and a synergy effect (increased etching rate as a result of successive chemical and physical steps). Although some promising results have been reported in development of ALE processes with particle beams for semiconductor industry, the introduction of ALE requires the capacity to implement such processes in scalable industrial plasma sources designed to process wafers with diameters up to 300 mm. Plasma approaches should provide high productivity, but they also have certain disadvantages: the lack of separation of ions by mass and energy, non-locality of exposure, etc. The energies of ions incident on the modified surface determine the possibility of heterogeneous ion-stimulated processes. These reactions are often threshold in nature.

A comprehensive approach combining several optimization directions is needed to expand the application of ALE in microelectronics with the use of plasma processes [2]. First, it is important to increase the processing rate while maintaining the self-limiting reaction mechanism that underlies ALE. Second, one needs to eliminate hot tails of the ion energy distribution in order to ensure low densities of defects introduced into the underlying semiconductor and dielectric structures. Third, narrowing of the energy spectrum of ions involved in etching is critically important, since this, coupled with a proper choice of chemical properties that modify the surface of films, ensures the efficiency of activation and helps avoid sputtering. All these tasks are closely tied to the need to obtain a controlled ion energy distribution function (IEDF). The ion energy profile determines how well the process fits the „ALE window“, a narrow energy interval within which the modified surface layer is removed completely while the unmodified material remains intact [2]. Even a slight deviation from this narrow energy range leads to parasitic physical sputtering, which induces the formation of structural defects and uncontrolled etching. This „window“ concept necessitates the production of a narrow IEDF, which allows for enhancing the synergy between the chemical and physical steps of the etching process with a simultaneous increase in the rate of processing of large-diameter wafers. It is worth noting that a narrow IEDF provides an opportunity to synthesize nanoscale structures with atomic precision and avoid parasitic physical sputtering.

In inductively coupled plasma (ICP) reactors, the energy spectrum of ions reaching the wafer surface is controlled by applying a radio-frequency (RF) bias voltage, which produces an electric field, to the substrate. This sinusoidal RF bias is applied to the substrate holder through a decoupling capacitor and produces a periodically changing electric field that forms a plasma sheath through which the accelerated ions move. The table inside the reactor chamber

(to which the substrate holder is secured) is charged negatively on average, since this balances the currents of hot electrons and relatively cold ions. In the positive half-period phase, ions are accelerated towards the substrate, forming a high-energy component of the spectrum. In the negative phase, the field is inverted, slowing the ions down and forming a low-energy component. Since the process is cyclic, two stable energy peaks emerge in steady-state operation. This is what lies behind the characteristic bimodal IEDF shape [1].

The ability to control IEDF in modern technological processes plays a critical role in minimizing defects that arise in nanomaterials. The role of IEDF in the mechanisms of pore sealing on the surface of dielectrics with ultra-low permittivity has been studied extensively in recent years [3,4]. This process is specific in that the surface layer (oxide, nitride, or metallic) is modified with low-energy ions and the embedded ions do not affect the permittivity value. It should be noted that the influence of ion mass on the rate and depth of penetration was also reported in these studies. Heavy low-energy ions modified the surface layer very quickly and uniformly, while light ions penetrated deeper. A narrow IEDF, which provides precise control over the process, is important here. This feature allows for minimization of random damage to the material under ion bombardment due to the limited energy spread, which, in turn, guarantees high reproducibility of the experimental results.

IEDF modeling serves as a tool for investigating the physical mechanisms that shape the energy profiles. In the present study, special attention is paid to particle dynamics both in the plasma sheath and at the interface with the processed material.

The dynamics of particles in the plasma sheath is examined within the drift-diffusion approximation that is characterized by the current density equation:

$$\bar{J} = q(\mu n\bar{E} - D\overline{\nabla n}), \tag{1}$$

where mobility $\mu = q/m\nu_{m,i}$, diffusion coefficient $D = kT_e/(m\nu_{m,i})$, $\nu_{m,i}$ is the ion transport frequency, T_e is the electron temperature, n is the electron density, q is the electron charge, m is the particle mass, and k is the Boltzmann constant. As was demonstrated in [5,6], the consideration of collisional processes is key to enabling the application of this approximation. The criterion of predominance of collisional processes over inertial ones needs to be satisfied for the drift-diffusion model to be applicable:

$$\nabla(nm\bar{V}\bar{V}) \ll nm\bar{V}\nu_{m,i}, \tag{2}$$

where $\bar{V}$ is the average velocity.

In practice, to align the theory with experimental data (especially in strong electric fields), one needs to take into account the dependence of mobility on ratio E/p, where p is pressure. This correction provides an opportunity to characterize more accurately the actual processes in the plasma sheath at high field E/p values.

With this aim in view, we performed plasma probe diagnostics first. These measurements provided data on key parameters, such as electron density (n_e) and temperature (T_e). The experiment is described in Section 1, and its results are reported in Section 3.1. These data became the basis for calibrating the developed hydrodynamic model, which reproduces the conditions of a low-pressure plasma discharge. This calibration ensured that the output parameters corresponded to actual experimental conditions, eliminating the need for in-depth modeling of the entire reactor. A description of the model is presented in Section 2. At the next stage, a need arose to introduce collisional processes in plasma, which necessitated the correction of ion mobility coefficients for preserving the applicability of the drift-diffusion approximation under low-pressure conditions. The results of mobility tuning in the model are detailed in Section 3.2. With the model set up, a parametric analysis of the influence of process parameters, which included the amplitude (V_{rf}) and frequency (ν_{rf}) of alternating bias voltage, the chamber pressure (p), the ICP discharge power (W_{icp}), and the gas mixture composition, on IEDF formation and silicon sputtering rate was performed. The results of analysis of these dependences are presented in Sections 3.3–3.5. It was found that the IEDF depends to a significant extent on the ion mass, the parameters of applied bias voltage, and the plasma composition, which is manifested in changes in the average ion energy and the distribution width. Particular attention was paid to the effect of adding Xe to Ar plasma, which led to changes in both the energy spectrum of ions reaching the surface and the sputtering rate. The obtained sputtering rate data were compared with experimental results, and the validity of the obtained patterns was confirmed. The results are detailed in Section 3.6.

1. Experiment

ICP diagnostics was carried out using a PlasmaLab 100 (OIPT, United Kingdom) plasma-chemical etching setup, which is an ICP reactor with a cylindrical chamber 380 mm in diameter and 450 mm in height. The chamber body is made of aluminum. Plasma was generated by a cylindrical copper spiral inductor positioned at a height of approximately 300–400 mm and operating at a frequency of 2 MHz. The inductor was kept in atmosphere and separated from the chamber volume by a cylindrical dielectric window made of vacuum ceramics based on aluminum oxide. The substrate to be processed (up to 200 mm in diameter) was positioned on the lower electrode at a distance of approximately 315 mm from the top of the reactor with a cooling system utilizing nitrogen or an antifreeze agent. A vacuum system with a turbomolecular pump with a residual vacuum of 10^{-7} Torr was used. Working gases were fed via mass flow regulators without interrupting the pumping process, while the pressure was controlled with a damper valve on the pumping line with an accuracy no worse than

± 0.1 mTorr. A constant total gas flow of 50 sccm was maintained in all experiments. The variable parameters were the generator power ($W_{icp} = 500-2500$ W), the pressure ($p = 5-20$ mTorr). and the composition of the gas mixture (Ar or Ar/Xe). The first series of experiments was focused on the study of Ar plasma with varying power and pressure levels.

In this argon plasma experiment, n_e and T_e were measured under the following conditions:

- the pressure in the chamber varying within the 5–20 mTorr range at constant power $W_{icp} = 800$ W;
- the ICP generator power varying within the 500–2500 W range at constant $p = 10$ mTorr.

The second series of measurements was carried out in Ar/Xe plasma at fixed power ($W_{icp} = 1500$ W) and pressure ($P = 10$ mTorr) levels and different fractions of xenon in the mixture.

The plasma characteristics were analyzed using a Langmuir probe (ESPion, Hiden Analytical, United Kingdom). A platinum probe 130 μm in diameter and 10 mm in length was chosen for pure argon plasma, and a tungsten probe 250 μm in diameter and 9 mm in length was used in experiments with the Ar/Xe mixture. The current–voltage curves (I-V curves), which had the form of a Maxwellian distribution within the range of 0–10 eV, were processed with preliminary correction for the ion current, which was determined using the orbital-motion-limited (OML) theory [7]. This allowed us to determine the electron temperature (T_e) and the electron density (n_e). As was found in subsequent calculations, the radii of both probes in the experiment were close in order of magnitude to the Debye length. Although this contradicts the classical assumptions of OML theory, it is known that it is satisfied for probe radius/Debye length ratios close to unity [8]. This is also confirmed by the root dependence of current on voltage in the ionic I-V part that was observed in our experiment: $I \sim V^{1/2}$.

In addition to plasma diagnostics, we conducted an experiment on silicon sputtering in plasma of the Ar/Xe mixture. The main objective was to examine the influence of the fraction of xenon in the plasma-forming mixture on the silicon sputtering rate. The plasma parameters were the same as those set in the second series of plasma diagnostics. The magnitude of DC bias applied to the substrate by the bias generator was adjusted individually for each Ar/Xe ratio in the plasma-forming mixture based on the data on average distribution energy E_{av} and plasma potential V_p, which were obtained in modeling, to produce an ion flux with the required energy on the substrate. At each experimental point, the processing time was varied within the range of 5–10 min to exclude the influence of substrate heating and other nonlinear effects and obtain reliable data on the sputtering rate. Three independent experiments were performed for each fraction of Xe in the Ar/Xe mixture in order to assess reproducibility. The samples were industrial silicon-on-insulator (SOI) wafers with the following structure: crystalline silicon (50 nm) / silicon oxide (200 nm) / single-crystal silicon substrate (750 μm). The thickness of the top silicon layer was measured before and after the sputtering experiment by spectral ellipsometry (with an error no greater than 0.2 nm). The advantage of working with such structures was that changes in the silicon layer thickness could be monitored with a high accuracy. The buried oxide layer had no effect on the plasma sheath voltage and on the ion distribution.

2. Model

A one-dimensional hydrodynamic model of plasma sheath, which is based on the modified drift-diffusion approximation and utilizes both thermal and drift velocity components [9], is implemented in the present study. The model was developed in COMSOL Multiphysics using the specialized Plasma module, which allows one to solve the balance equations of charged particles and energy within the diffusion-drift approximation.

In the inductively coupled plasma model, the input power is distributed uniformly in space. It is worth noting that this assumption of a uniform power distribution is a simplification. However, the focus of the present work is on the near-surface effects governed by the applied RF bias, and the averaged volumetric plasma parameters were set in accordance with probe diagnostics data from the reactor center. The power parameter value is chosen in such a way as to correspond to the measured values of electron density and temperature obtained as a result of probe diagnostics. To control the energy spectrum of ions on the substrate surface, an independent generator of alternating bias voltage

$$V = V_{rf} \cos(2\pi \nu_{rf} t) \tag{3}$$

with adjustable ν_{rf} and V_{rf} is included in the model; it sets a boundary condition simulating a DC-isolated electrode. The opposite boundary of the model corresponds to the grounded wall of the reactor. The mechanism of formation of bias voltage and its influence on the average energy and width of ion distribution were discussed in detail in our earlier study [10]. It is worth noting that the DC self-bias arising from the difference in electrode areas in real asymmetric reactors is neglected in the present study, which is reflected in the symmetric geometry of the model and the dominant influence of the RF bias voltage on IEDF. Here, we evaluate qualitatively the influence of discharge parameters, such as pressure, composition, power input into the discharge, etc., on the ion energy distribution function in a one-dimensional model; the results are more relevant at bias voltages of several tens of volts.

The system of equations characterizing the generation and dynamics of plasma includes:

1) continuity equations for electrons, ions, and neutrals;

2) Poisson equation for calculating the self-consistent electric field;

3) energy balances that take into account the motion of particles in an electromagnetic field and their collisional losses.

The official COMSOL documentation provides additional in-depth data [11], and the relevant implementation specifics were discussed in [9]. The cross sections of elastic and inelastic collisions of electrons with argon (Ar) and xenon (Xe), which include reactions of elastic scattering, excitation, ionization of neutral atoms, stepwise ionization, and chemical (Penning) ionization [12–15], ensure the physical validity of modeled processes. The boundary conditions at the reactor walls included the reactions leading to loss of ionized and excited states in Ar gas plasma taken from [16]; similar conditions were also applied in the case of Xe [6,14,17,18].

The model was improved by including a correction for ion mobility in the diffusion-drift approximation. This made it possible to introduce nonlinear effects within a wide range of electric fields with minimal computational costs, which is confirmed by the agreement of the obtained results with experimental data [5]. It is worth noting that this approach does not necessarily provide a more accurate description of processes in plasma sheath than the momentum transfer equation, but it reveals the trends affecting IEDF, which are discussed in the present paper. The mobility was calculated as a function of the electric field strength using the following formula [5]:

$$\mu_y(E) = \frac{\mu_{y,0}}{(1 + AE/p)^{1/2}}, \tag{4}$$

where $\mu_{y,0}$ is the mobility in zero electric field (subscript y denotes the gas particle type: Ar or Xe), A is a constant used to fit simulation results to experimental data, p is the pressure, and E is the electric field strength. Formula (4) accounts for two possible modes: the one observed when the thermal velocity of particles exceeds the drift velocity, which is typical of weak electric fields, and the one arising when the drift velocity of ions prevails over the thermal velocity. In other words, the formula yields a constant mobility at low values of the reduced electric field strength and switches to a dependence inverse to the square root of the field when the field grows more intense. With the drift velocity taken into account, the frequency of ion collisions in an electric field increases, suggesting that the collisional term in the equation of ion motion is significant compared to the inertial one [18]. The mobility in zero electric field was calculated as

$$\mu_{y,0} = \frac{q}{m\nu} = \frac{q}{\frac{p}{kT_g} m\sigma \sqrt{\frac{8kT_g}{\pi m}}} = \frac{q}{p\sigma \sqrt{\frac{8m}{kT_g \pi}}}, \tag{5}$$

where T_g is the gas temperature and σ is the cross section of collisions of ions with neutral particles. An important aspect of the study was the identification of discrepancies between the calculated and experimental values of electron temperature obtained by probe diagnostics. When the model was parameterized, the theoretical estimate of ion mobility led to a two-fold underestimation of T_e in both pure gases and their mixtures. Apart from this T_e discrepancy, the variation of constant A in the gas mixture was found to result in uncertainty in ion fluxes reaching the wafer. To eliminate this uncertainty and the T_e discrepancy, we analyzed the influence of three key parameters incorporated into the model: ion mobility $\mu_{y,0}$, constant A, which regulates the dependence of mobility on electric field strength E, and equivalent power W_{icp}. This was done by varying the parameters listed above in such a way that their effect on the model could be identified.

The use of Eq. (4) ensures the satisfaction of the model's applicability criteria under low-pressure conditions and provides an opportunity to extrapolate it beyond the initial pressure limits (< 10 mTorr) [11], since the modified mobility proposed here makes an allowance for both drift u_d and thermal u_{th} velocities. The averaged collision frequency takes the form

$$\nu_{m,i} = \frac{\sqrt{\frac{3}{2} u_{th}^2 + u_d^2}}{\lambda_{\text{MFP}}}, \tag{6}$$

where λ_{MFP} is the mean free path. The drift velocity in a strong electric field E is defined as

$$u_d = \sqrt{\frac{q\lambda_{\text{MFP}}}{m_i} E}, \tag{7}$$

where m_i is the ion mass. This is attributable to the fact that the drift velocity of particles in strong electric fields is significantly higher than the thermal velocity. It is worth noting that the mobility formula was found in [5] by the Wannier method. Within this approach, the formula for the collision frequency takes the following form:

$$\nu_{m,i} = \frac{\sqrt{\frac{3}{2} u_{th}^2 + u_d^2}}{\lambda_{\text{MFP}}} = \frac{\sqrt{\frac{3}{2} \frac{8KT_i}{\pi m_i} + \frac{q\lambda_{\text{MFP}}}{m_i} E}}{\lambda_{\text{MFP}}} = \frac{\sigma_{i,p} P}{KT_g} \sqrt{\frac{12KT}{\pi m_i} + \frac{qKT_i}{m_i \sigma p_x} E}, \tag{8}$$

where p_x is the momentum.

The ion energy distribution function is calculated by the particle tracing method in a self-consistent electric field defined through the potential gradient: $E = -\nabla V$. The initial ion velocities are set randomly in accordance with a Maxwellian distribution averaged at distance $z = 15.5$ cm from the substrate. The particle dynamics is modeled by the equations of motion:

$$\Delta V_i = \frac{qE(t)}{m} \Delta t, \tag{9}$$

$$V_{i(new)} = V_{i(old)} + \Delta V_i, \tag{10}$$

$$\Delta X = V_{i(new)} \Delta t, \tag{11}$$

where Δt is the time step and V_i is the ion velocity. Following the collision of an ion with the surface, its kinetic energy was recorded and added to the overall distribution.

Tracing was performed under the following additional conditions:

• number of traced particles: $N = 500-2000$ (chosen depending on RF bias frequency ν_{rf}). Numbers $N > 2000$ provide noise smoothing only, while the influence on the IEDF shape is marginal;

• time step: from $t = 2.5 \cdot 10^{-10}$ s (for $\nu_{rf} = 2$ MHz) to $6.66 \cdot 10^{-11}$ s (for $\nu_{rf} = 30$ MHz) $7.4 \cdot 10^{-11}$ s. In most experiments, frequency $\nu_{rf} = 13.56$ MHz and time step $7.4 \cdot 10^{-11}$ s were used.

Since the mean free path of ions is large ($\lambda_{\text{MFP}} > d_p$, where d_p is the size of plasma sheath), collisions of ions with neutrals were not taken into account in the IEDF calculation. However, it is worth noting that spatiotemporal dependence $E(x, t)$ incorporates the contribution of collisional processes through changes in the plasma potential.

The IEDF calculation is performed after reaching a steady state, which is identified by the stabilization of the following parameters: electron and ion density, electron temperature, ion and electron flux to the surface, and bias voltage. The criterion of stationarity was the lack of any changes or, where changes are attributable to the influence of the bias voltage, such changes induced within 0.1 s.

Sputtering rate S_Y is defined as

$$S_Y = Y\Gamma_{i,y}, \tag{12}$$

where $\Gamma_{i,y}$ is the flux of ions type y to the surface. It should be noted that $\Gamma_{i,y}$ was estimated in accordance with the approach outlined in [19] for the plasma sheath. The ion density at the plasma sheath was calculated as the electron density in the center of the reactor divided by the base of natural logarithm. In accordance with [19], the ion velocity at this boundary was taken to be approximately equal to the Bohm velocity multiplied by a factor of 1.6, and the resulting flux was calculated as the product of density and velocity.

Sputtering coefficient Y was introduced in order to evaluate the effect of the ion flux on the surface of the wafer being processed. It depends on the IEDF and is defined as the ratio of the number of atoms leaving the sample it to the number of incident ions:

$$Y = \Sigma_E Y_{E,y} N_{E,y} / N_{N,y}. \tag{13}$$

Here, $Y_{E,y}$ is the energy-dependent sputtering coefficient for ions type y taken from the experimental data [20], $N_{E,y}$ is the number of ions with energy E, and $N_{N,y}$ is the total number of ions type y. It is worth noting that a significant contribution of metastable states and vacuum UV radiation to sputtering in an experiment with argon and xenon ions with low energies ($E < 100$ eV), which may affect the obtained sputtering rate data, was reported in [20].

A complete description of the developed hybrid model, which combines hydrodynamic calculation of plasma parameters and kinetic modeling of the ion energy distribution function, is presented in Fig. 1. The model includes:

1) probe diagnostics;

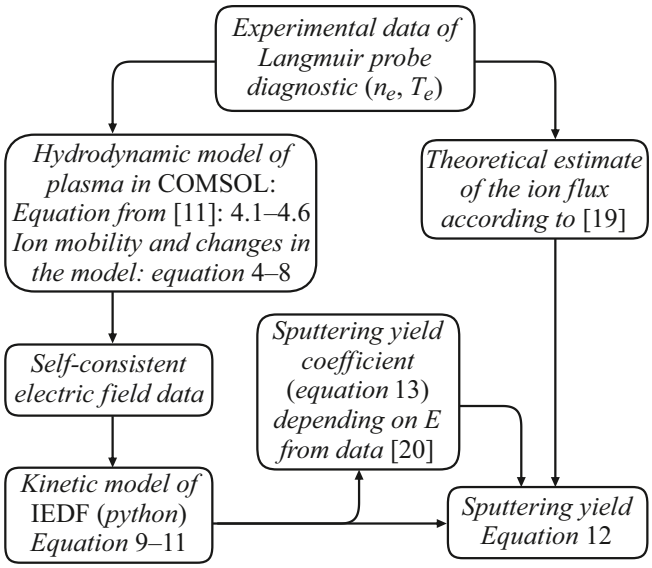

Figure 1. Diagram of the model.

2) COMSOL hydrodynamic block with modified ion mobility;

3) kinetic block for particle tracing in a self-consistent field;

4) sputtering rate calculation.

3. Results

The developed model, which was implemented in the COMSOL software package using a specialized module for particle tracing in a self-consistent electric field (written in Python), allowed us to conduct a comprehensive analysis of the influence of key plasma parameters on the IEDF and the silicon sputtering rate. This model relies on a hydrodynamic description of the plasma sheath with account for the modified ion mobility based on the experimental T_e and n_e values, which are the input data of the model.

3.1. Experimental data

The results of probe measurements are shown in Fig. 2. Figure 2, *a* presents the dependence of T_e and n_e on pressure within the 5–20 mTorr range. As the pressure increases, the electron density is seen to increase linearly from $1.1 \cdot 10^{11}$ to $2.5 \cdot 10^{11}$ cm^{-3}. At the same time, the electron temperature decreases from 3.05 to 2.5 eV, which is attributable to an increase in frequency of electron-atom collisions and the loss of energy by electrons.

Figure 2, *b* illustrates the influence of the generator power on the plasma parameters. When the power increases from 500 to 2500 W, T_e grows only slightly from 2.68 to 3.33 eV, while n_e increases almost proportionally to power from $1.0 \cdot 10^{11}$ to $3.2 \cdot 10^{11}$ cm^{-3}. This power rise results in an increase in energy transferred to electrons

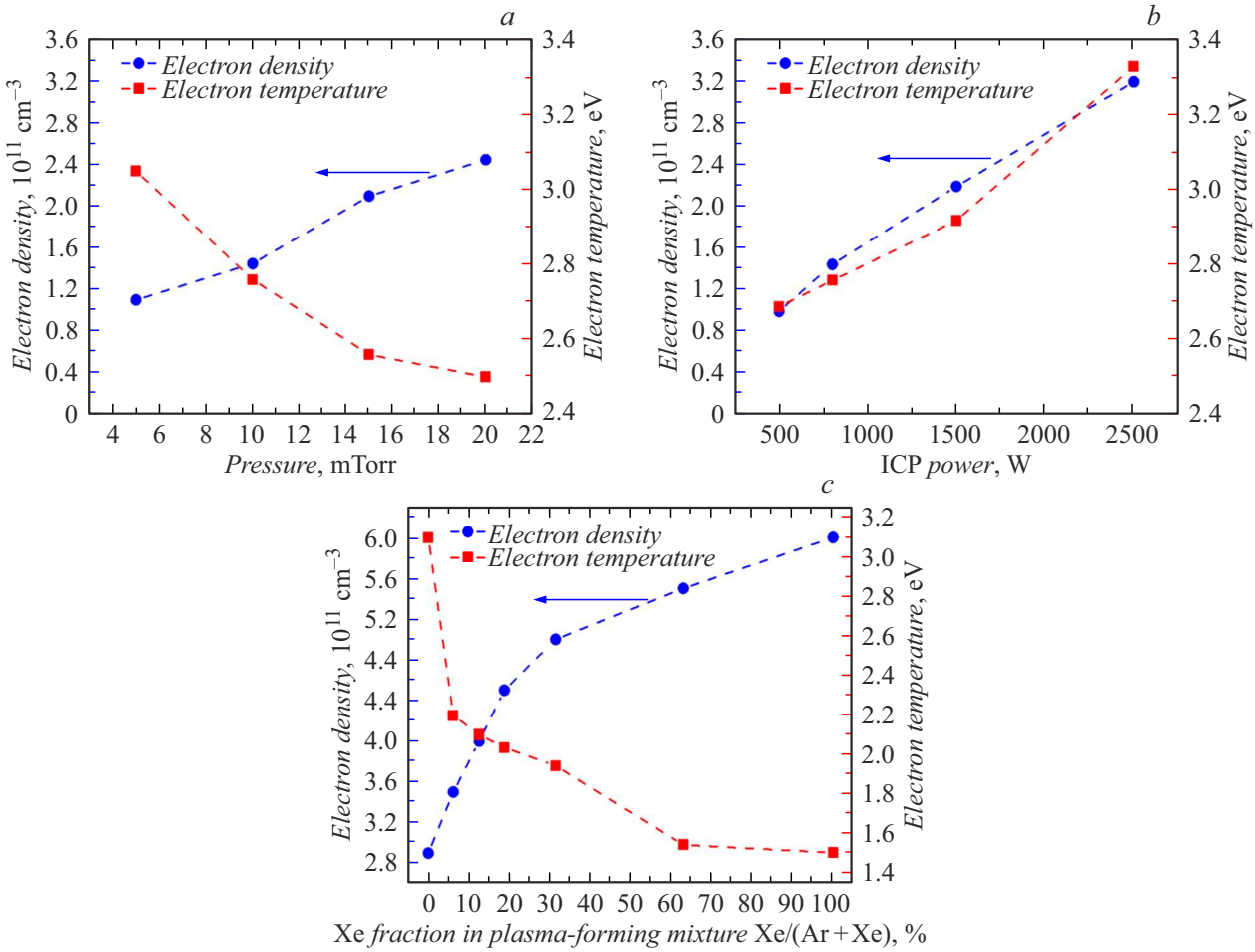

Figure 2. T_e and n_e as functions of: *a* — pressure in the chamber at $W_{icp} = 800$ W; *b* — ICP power at $p = 10$ mTorr; *c* — fraction of Xe in the plasma-forming mixture at $p = 10$ mTorr, $W_{icp} = 1500$ W.

by the RF field, enhancing ionization and, consequently, increasing slightly the electron temperature.

Figure 2, *c* illustrates the effect of increasing the fraction of xenon in the plasma-forming Ar/Xe mixture. At a Xe percentage up to 6.2%, T_e drops sharply from 3.1 to 2.2 eV due to the fact that the xenon ionization energy is lower, which shifts the ionization balance toward Xe^+. As the Xe percentage increases further (> 30%), the growth of n_e slows down (from $5.0 \cdot 10^{11}$ to $6.0 \cdot 10^{11}$ cm^{-3}).

3.2. Mobility adjustment

As was already noted, to eliminate the ion flux uncertainty and the T_e discrepancy, one needs to analyze the influence of three key parameters incorporated into the model: ion mobility $\mu_{y,0}$, constant A, which regulates the dependence of mobility on electric field strength E, and equivalent power W_{icp}. Simulated data revealed that the measurement of input power W_{icp} without adjustment of the other parameters resulted in a strong variation of ion density (n_e increases with W_{icp}), but had almost no effect on the electron temperature. When parameter $\mu_{y,0}$ was varied and the other parameters were kept unchanged, mobility was found to affect T_e (T_e increases with $\mu_{y,0}$), but had negligible influence on the ion density. In turn, parameter A helps fit the ion fluxes to the experimental data when $\mu_{y,0}$ and W_{icp} in the model are chosen so as to obtain the needed T_e and n_e. It is worth noting that parameter $\mu_{y,0}$ for gas mixtures was varied for each ion type in such a way as to maintain the original $\mu_{\mathrm{Ar},0}/\mu_{\mathrm{Xe},0}$ ratio obtained in theoretical calculations. The main difficulty was in varying parameter A in gas mixtures: it was discovered that this parameter may affect the ratio of ion fluxes, which is why it was necessary to minimize its influence. It was found in calculations that parameters $\mu_{y,0}$ and W_{icp} in the model must be minimized in order to achieve the required T_e while maintaining n_e. This approach allowed us to vary parameter A arbitrarily while exerting almost no influence on the ion flux attributable to this variation of A. Thus, when parameter A was varied within the range from 0 to 10^{33} Pa·m/V, the spread of fractions of ions of each type did not exceed 1% if the plasma-forming mixture contained no more than 50% Xe; with

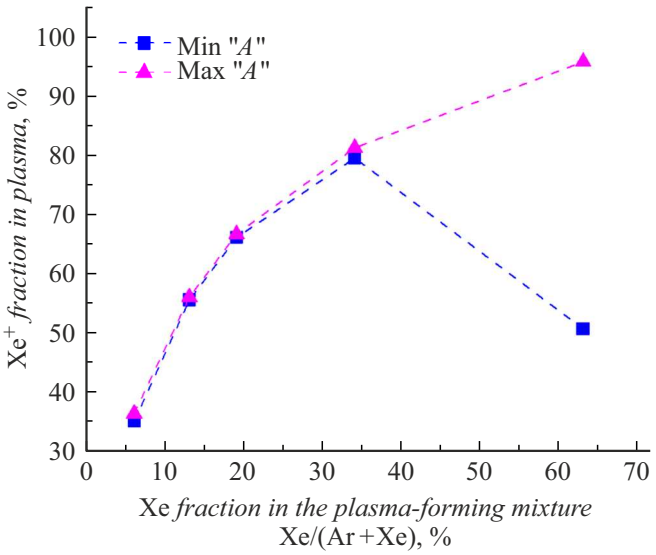

Figure 3. Xe^+ fraction in plasma as function of the initial Xe fraction in the plasma-forming mixture at $p = 10$ mTorr and $W_{icp} = 1500$ W. Parameter A is varied with the required T_e and n_e values being maintained.

a higher percentage of xenon, the error increased (see Fig. 3). Mobility $\mu_y(E)$ varied in this case within the range from 0 to $\mu_{y,0}$. It is worth noting that this fitting algorithm typically allowed us to obtain the experimental values of T_e by varying only two of the three parameters without affecting the other properties of plasma as a whole.

The IEDF and sputtering rate analysis revealed only a very weak influence of $\mu_{y,0}$ on the average distribution energy ($E_{av} < 1$ eV) and the distribution width ($\Delta E < 2$ eV) after fitting performed to meet the specified requirements. The end result of determination of the sputtering rate demonstrated that mobilities $\mu_{y,0}$ have virtually no effect on the sputtering rate if the $\mu_{Ar,0}/\mu_{Xe,0}$ ratio obtained in theoretical calculations is equal to that obtained. At the same time, when mobilities $\mu_{y,0}$ increase at constant $\mu_{Ar,0}/\mu_{Xe,0}$, the spread of flux fractions of ions of one type onto the wafer also increases, which is why the minimum values of $\mu_{y,0}$ needed to obtain the desired T_e were used. When coefficients $\mu_{Ar,0}$ and $\mu_{Xe,0}$ were adjusted for each gas, the original ratio of these coefficients obtained in the theoretical calculation of $\mu_{y,0}$ by formula (5) with the use of cross section data [11,12,21] at gas temperature $T_g = 560$ K was also maintained. The need for mobility correction in the determination of theoretical mobility was discussed in [6]. A $\sim 2-3$-fold increase in $\mu_{y,0}$ relative to theoretical estimates was needed to obtain the electron temperature and density values measured experimentally. This increase provided close agreement with experimental data, confirming the robustness of the model to parameter variations.

3.3. Ar and Ar/Xe plasma

When both single-component Ar gas and Ar/Xe gas mixture plasmas were modeled, standard spatial distributions of the densities of gas particles and electrons were obtained (see Fig. 4, *a*, which presents the example of an Ar/Xe gas mixture with 13 % Xe in the plasma-forming mixture under zero bias). It is evident from Fig. 4, *a* that the density in the center corresponds to the data of probe diagnostics and the plasma itself is quasi-neutral. The gas mixture also shows the distribution of Ar ion and Xe ion densities, which combine to illustrate the spatial distribution of ions.

The region of the plasma sheath (near the electrode) in Fig. 4, *a* is shown in more detail in Fig. 4, *b*, which presents this region in approximation. This figure also illustrates the dependence of electron n_e and ion n_i densities in the sheath on bias voltage amplitude V_{rf}. It is evident that the space charge region expands with an increase in V_{rf}, which is attributable to an increase in electric field strength in the sheath. This field disrupts the quasi-neutrality of plasma by separating charged particles: electrons are pushed into the bulk, while ions are concentrated near the electrode.

Figure 5 presents the simulated distribution of electric potential in the reactor, illustrating the influence of alternating voltage amplitude on the dynamics of the system. The model is constructed so that the left wall ($x = 0$) is exposed to a sinusoidal signal with an amplitude of 5 V, while the right wall ($x = 315$ mm) is grounded. The results of analysis of the influence of signal amplitude suggest that the spatial structure of the potential distribution is preserved when the bias voltage fluctuates.

The time dependence of potentials at the electrode and in the center of the reactor at $V_{rf} = 50$ V is shown in Fig. 6, *a*. Within a negative V_{rf} half-wave, the potential in the center is limited by the plasma potential, since electrons, being highly mobile, screen the field instantly. Within a positive V_{rf} half-wave, the potential in the center mirrors the characteristics of the electrode potential, since massive ions cannot keep pace with rapid variations of the radio-frequency field.

Figure 6, *b* demonstrates the effective bias voltage generated in the model. The asymmetry of observed oscillations is attributable to the difference in mobility of electrons and ions; owing to this, positive and negative half-waves are screened differently by the charge that ends up in plasma sheath. The obtained results are consistent with the data from [1], where a similar asymmetry was observed experimentally.

3.4. IEDF modeling results in Ar plasma

The simulation results revealed (Figs. 7, *a, b*) that the amplitude of bias voltage V_{rf} has a significant effect on the IEDF. With V_{rf} increasing from 5 to 100 V, average ion energy E_{av} grows linearly, while distribution width ΔE increases almost linearly. This is associated with an increase in electric field strength E in the d_p sheath, which accelerates ions and reduces the time of their transit through

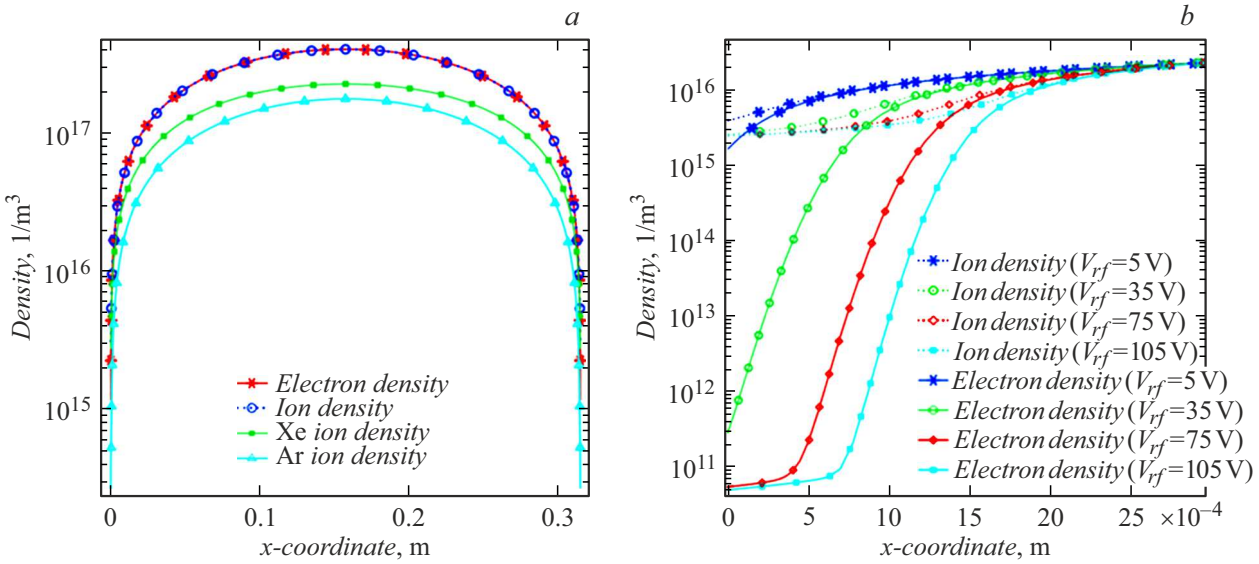

Figure 4. Distribution of the electron and ion density at $p = 10$ mTorr, $W_{icp} = 1500$ W: *a* — as a sum of the densities of Ar and Xe ions; *b* — in the plasma sheath as a function of bias voltage at $\nu_{rf} = 13.56$ MHz.

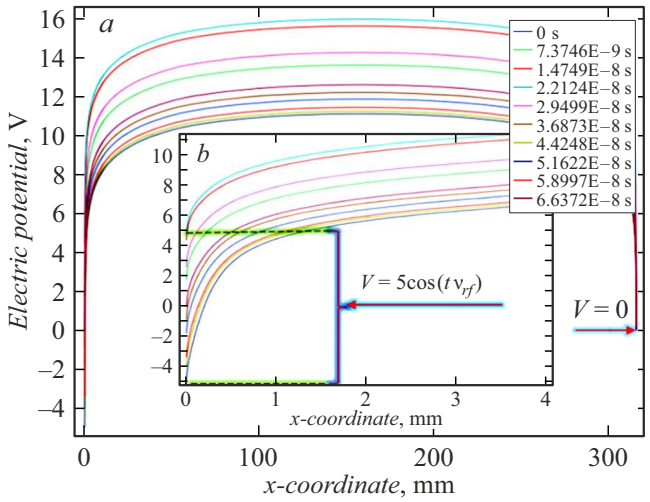

Figure 5. Distribution of the electric potential at $p = 10$ mTorr, $W_{icp} = 1500$ W, $V_{rf} = 5$ V, and $\nu_{rf} = 13.56$ MHz within a single period: *a* — over the reactor length in Ar plasma; *b* — approximation in the plasma sheath region.

the sheath. A shorter ion transit time and a change in acceleration in the plasma sheath cause an expansion of the IEDF. Input bias power $W_b < 1\,\%$ of W_{icp} does not affect the plasma parameters in the chamber volume, which verifies the local nature of V_{rf} influence.

The variation of IEDF with frequency ν_{rf} reveals strong changes in distribution width ΔE with a weak change in E_{av}. Figures 7, *c, d* illustrate the variation of IEDF with frequency ν_{rf} at a constant bias voltage amplitude V_{rf}. As ν_{rf} increases from 2 to 13.56 MHz, the distribution width decreases by 20 %–50 % with an additional variation of bias voltage and pressure due to averaging of the ion energy over the oscillation period. The sharp E_{av} drop at frequencies $\nu_{rf} > 13.56$ MHz is attributable to the inertia of ions, which do not have enough time to respond effectively to rapid electric field variations in the plasma sheath with a gradual increase in ν_{rf}. At even higher frequencies, the nature of ion motion changes, since, owing to high inertia, their behavior is determined not by instantaneous fluctuations of the field, but by its average effect. This contributes to the stabilization of E_{av} and is consistent with the data reported in [22].

An increase in ICP generator power W_{icp} from 500 to 2500 W causes a proportional increase in plasma density n_e, but electron temperature T_e increases by 25 % only. This, in turn, leads to an increase in ionization frequency and a change in the ratio of collisions of electrons with ions and neutral atoms, which contributes to a slight (less than 10 %) E_{av} reduction (Figs. 7, *e, f*). In addition, the IEDF width increases by 30 % due to a plasma sheath size change associated with the Debye length change within the Child–Langmuir law, the applicability of which to the RF sheath was discussed in [1]. Owing to the disproportionality of n_e and T_e, shortening of the Debye length leads to an approximately 2-fold change in the sheath size.

The influence of pressure p is manifested a little differently: with p increasing from 5 to 20 mTorr (Figs. 7, *g, h*), only a weak pressure dependence of E_{av} and ΔE was found in modeling. This is attributable to the fact that the particle density in plasma increases with pressure, leading to an increase in frequency of collisions of electrons with neutral atoms and ions. The electron temperature decreases slightly as a result, but the plasma density increases significantly, and, as a consequence, the plasma sheath becomes thinner. This is what explains the broadening of IEDF with increasing pressure, and the average energy is reduced due to collisional losses in the sheath.

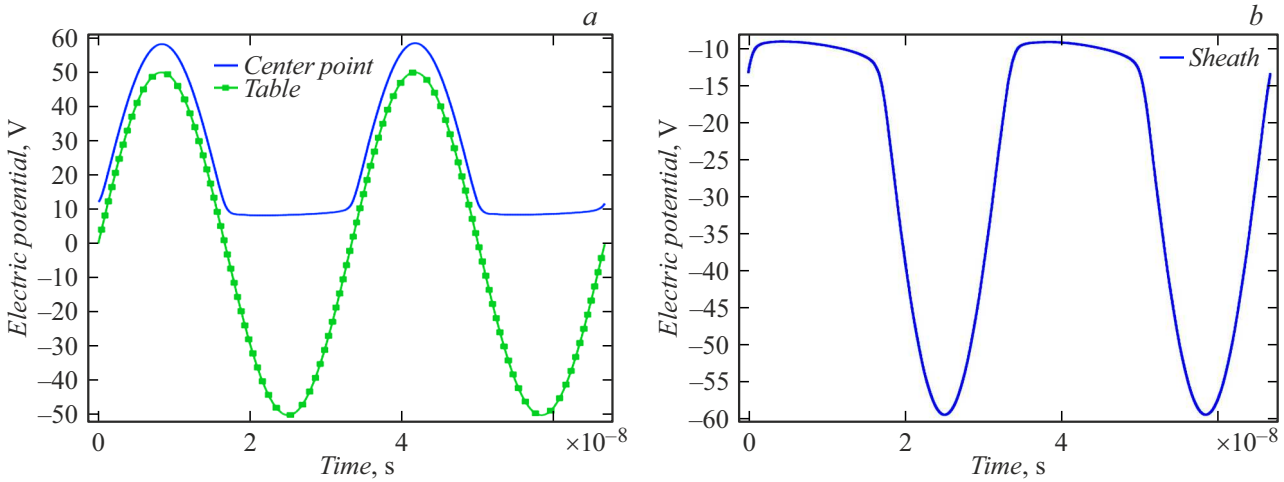

Figure 6. Distribution of the bias voltage at $p = 10$ mTorr, $W_{icp} = 1500$ W, $V_{rf} = 50$ V, and $\nu_{rf} = 30$ MHz: *a* — applied to the table with the sample and in the center of the chamber; *b* — in the plasma sheath.

3.5. IEDF modeling results in Ar/Xe plasma mixture

The introduction of xenon into argon plasma (Figs. 8, 9) revealed significant differences in the behavior of light Ar^+ argon ions and heavy Xe^+ xenon ions. The addition of xenon to argon plasma leads to IEDF broadening from 20 to 34 eV for Ar^+ and from 10 to 22 eV for Xe^+ (depending on the fraction of Xe in the plasma-forming mixture) due to the difference in ionization energy and an increase in electric field strength in the sheath. It is worth noting that Xe^+ ions have a narrower energy distribution, since they are heavier than Ar^+ ions in gas mixture plasma. As for the equality of the IEDF width for pure Xe and Ar gas plasma, narrowing of the spectrum due to the mass of Xe^+ ions is offset by a thinner sheath and a higher field strength in the sheath resulting from a change in Debye length. Figure 8, *b* also makes it evident that the distribution width dips around 20 % Xe in the plasma-forming mixture, since the ion flux is redistributed in favor of Xe^+ ions (Fig. 9, *a*), which is combined with a change in electron temperature and density.

The dynamics of ion fluxes (Fig. 9, *a*) has a nonlinear dependence on the composition of the gas mixture:

- Ar^+ flux drops sharply from $45 \cdot 10^{15}$ cm^{-2}·s^{-1} (pure Ar) to $19 \cdot 10^{15}$ cm^{-2}·s^{-1} at 20 % Xe and continues decreasing linearly to $3 \cdot 10^{15}$ cm^{-2}·s^{-1} (63 % Xe);
- Xe^+ flux increases fairly rapidly from $10 \cdot 10^{15}$ cm^{-2}·s^{-1} (6 % Xe) to $28 \cdot 10^{15}$ cm^{-2}·s^{-1} (36 % Xe), which is followed by weak linear growth from 28 to $37 \cdot 10^{15}$ cm^{-2}·s^{-1} at Xe fractions in the plasma-forming mixture exceeding 35 %.

This behavior may be attributed to the competition of processes affecting the flux of charged particles. With small additions of Xe (< 20 %), the suppression of Ar ionization dominates due to the lower ionization potential of Xe and a sharp T_e reduction, which has a negative effect on the generation of Ar^+. When more than 35 % Xe are added, the flux change gets saturated, which is attributable to a smoother variation of plasma parameters and the prevalence of Xe^+ in the overall ion flux (more than 80 %).

In turn, precise adjustment of the energy spectrum through variation of the gas mixture composition actually allows one to control the sputtering parameters. Silicon sputtering coefficient Y (Fig. 9, *b*), which characterizes the probability of sputtering a silicon atom by a single ion was obtained by interpolating the experimental data on the energy dependence of silicon sputtering from [20] and modeled by IEDF, increases for both Xe^+ and Ar^+. However, Y_{Ar} is ≈ 1.7 times higher than Y_{Xe} due to the fact that Ar^+ transfers energy to silicon atoms more efficiently, since the ratio of their masses is closer to the optimal one for maximum transfer [23] and Ar^+ has a higher velocity. The sputtering rates (Fig. 9, *c*) demonstrate opposite dependences on the Xe fraction in the plasma-forming mixture (i.e., the reduced contribution of Ar^+ is compensated for by an increase in Xe^+ flux, but the overall rate drops by a factor of almost 2, since Y_{Xe} is smaller). The sputtering rate for Xe^+ increases ≈ 2.2 times when 20 % Xe are added, which is attributable to a reduction in plasma potential and T_e and an increase in n_e. The maximum rate is achieved for pure Ar ($\approx 1.5 \cdot 10^{14}$ atom/cm^2·s), which is crucial for low-energy processes. However, it is worth noting, that this sputtering maximum is associated with additional damage to the underlying material due to the wide distribution function.

3.6. Comparison of the results of simulation and experiment in Ar/Xe plasma mixture

Figure 10 presents the results of a comparative analysis of data on the sputtering rate of silicon (Si) in plasma of the argon–xenon gas mixture obtained by modeling and in the experiment performed using the plasma-chemical

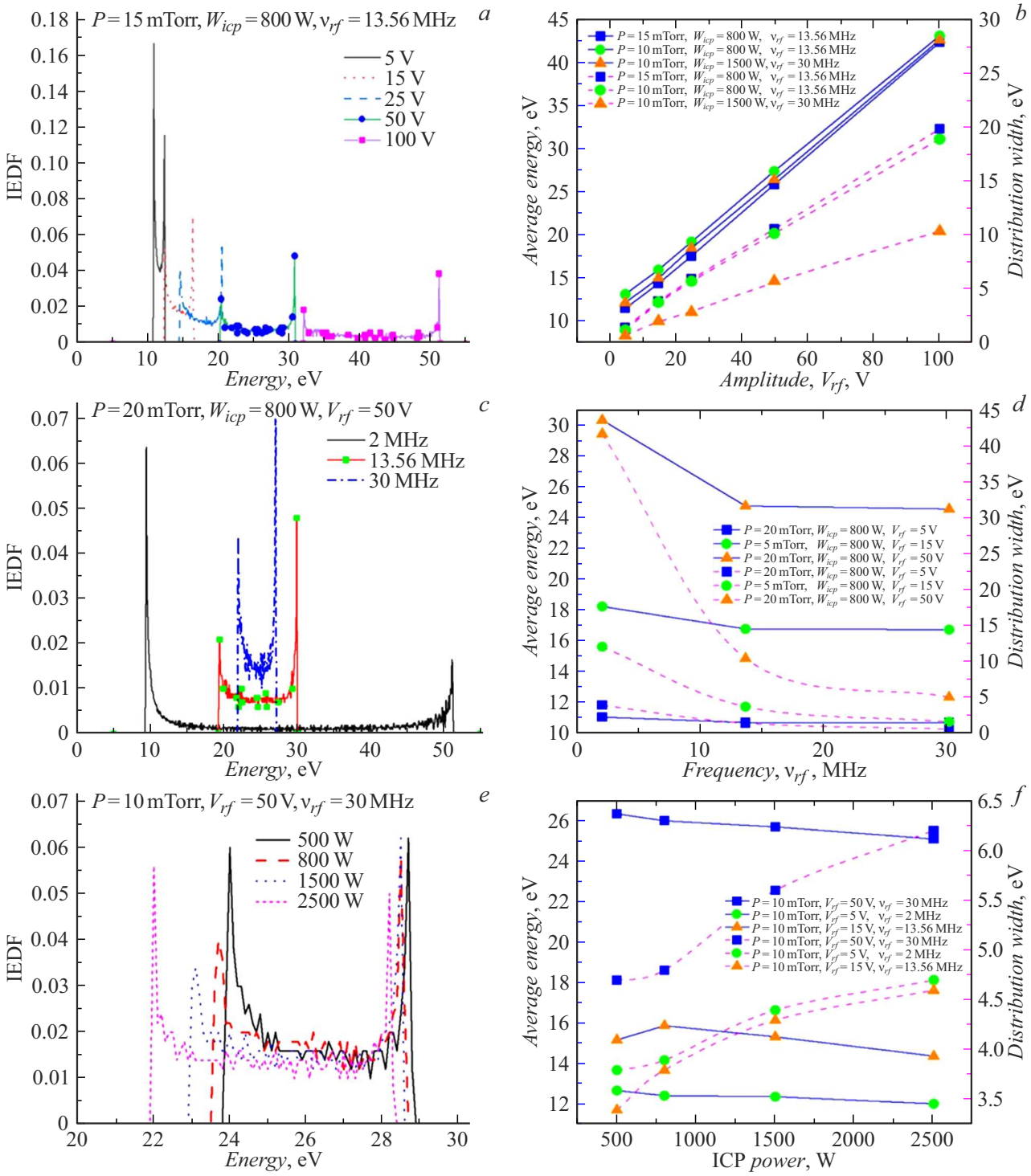

Figure 7. Ion energy distribution functions: *a* — at $p = 15$ mTorr, $W_{icp} = 800$ W, and $\nu_{rf} = 13.56$ MHz; *b* — plotted versus V_{rf} at different discharge parameters; *c* — at $p = 20$ mTorr, $W_{icp} = 800$ W, and $V_{rf} = 50$ V; *d* — plotted versus ν_{rf} at different discharge parameters; *e* — at $p = 10$ mTorr, $\nu_{rf} = 30$ MHz, and $V_{rf} = 50$ V; *f* — plotted versus W_{icp} at different discharge parameters; *g* — at $W_{icp} = 800$ W, $\nu_{rf} = 13.56$ MHz, and $V_{rf} = 100$ V; *h* — plotted versus p at different discharge parameters.

etching setup. The simulation reveals a stable trend: the Si sputtering rate decreases as the fraction of Xe in the plasma-forming mixture increases (specifically, the rate goes down from 0.4 arbitrary units (a. u.) at a minimum xenon concentration to 0.2 a. u. at a high Xe concentration). The experimental data are indicative of a similar dependence, but a sharper drop in sputtering rate is observed with the addition of less than 20 % Xe; this is not reproduced fully by

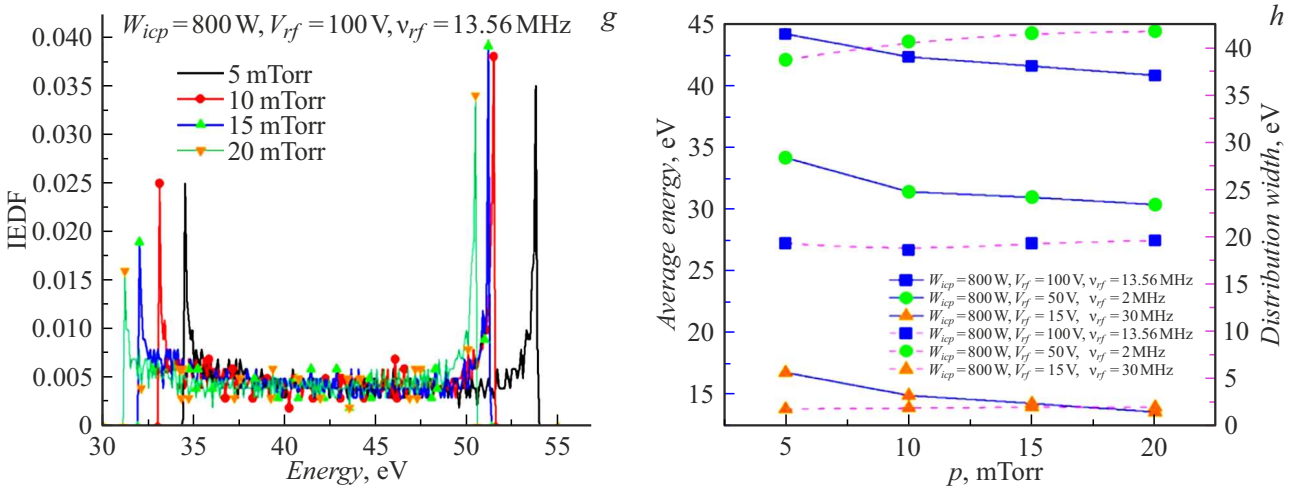

Fig. 7 (*Contd.*).

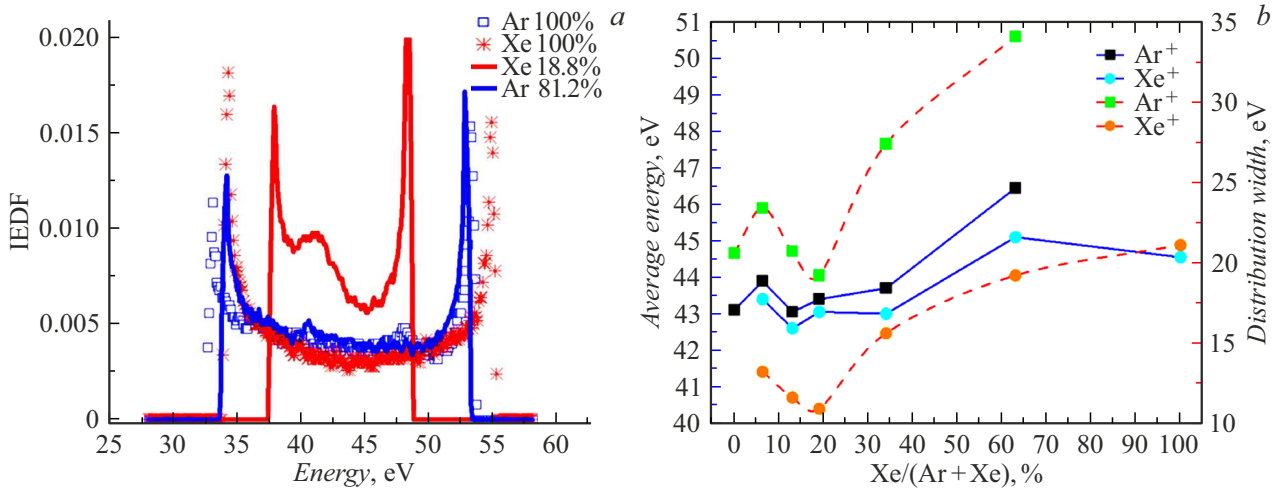

Figure 8. *a* — IEDF in Ar/Xe mixture plasma and IEDF of pure gases; *b* — average energy and distribution width plotted versus the fraction of Xe in the plasma-forming mixture at constant parameters of the discharge and the bias voltage.

the model. This discrepancy may be attributed to limitations of the model, which does not take into account a number of physical effects, such as the influence of vacuum ultraviolet radiation, the contribution of metastable states to sputtering (see earlier study [20]), and lack of consideration of DC self-bias, and to the difficulty of measurement of actual ion fluxes onto the wafer surface in the reactor chamber, which are needed to calculate the sputtering rate based on the IEDF simulation results (this is why the sputtering rate is given in arbitrary units). It should also be taken into account that different setups may produce different contributions to sputtering rates. The sputtering rate reduction with an increase in Xe fraction is explained by changes in the composition and the energy characteristics of ions in the plasma: heavy xenon atoms reduce the efficiency of energy transfer by ions to the Si surface, which leads to suppression of the sputtering process.

Conclusion

The study demonstrated the possibility of controlling IEDF through bias voltage, pressure, and power of the ICP generator for optimization of plasma etching processes in micro- and nanoelectronics. The developed hybrid model, which combines a hydrodynamic description of the plasma sheath in COMSOL Multiphysics and a kinetic particle tracing method implemented in Python, allowed for a systematic analysis of the influence of process parameters on the ion energy spectrum and the sputtering rate in inductively coupled plasma. The model was verified against experimental data of probe diagnostics and provided an opportunity to obtain IEDFs allowing one to estimate the surface sputtering rate, provided that data on the experimental ion fluxes reaching the surface are available to achieve qualitative agreement with the experiment.

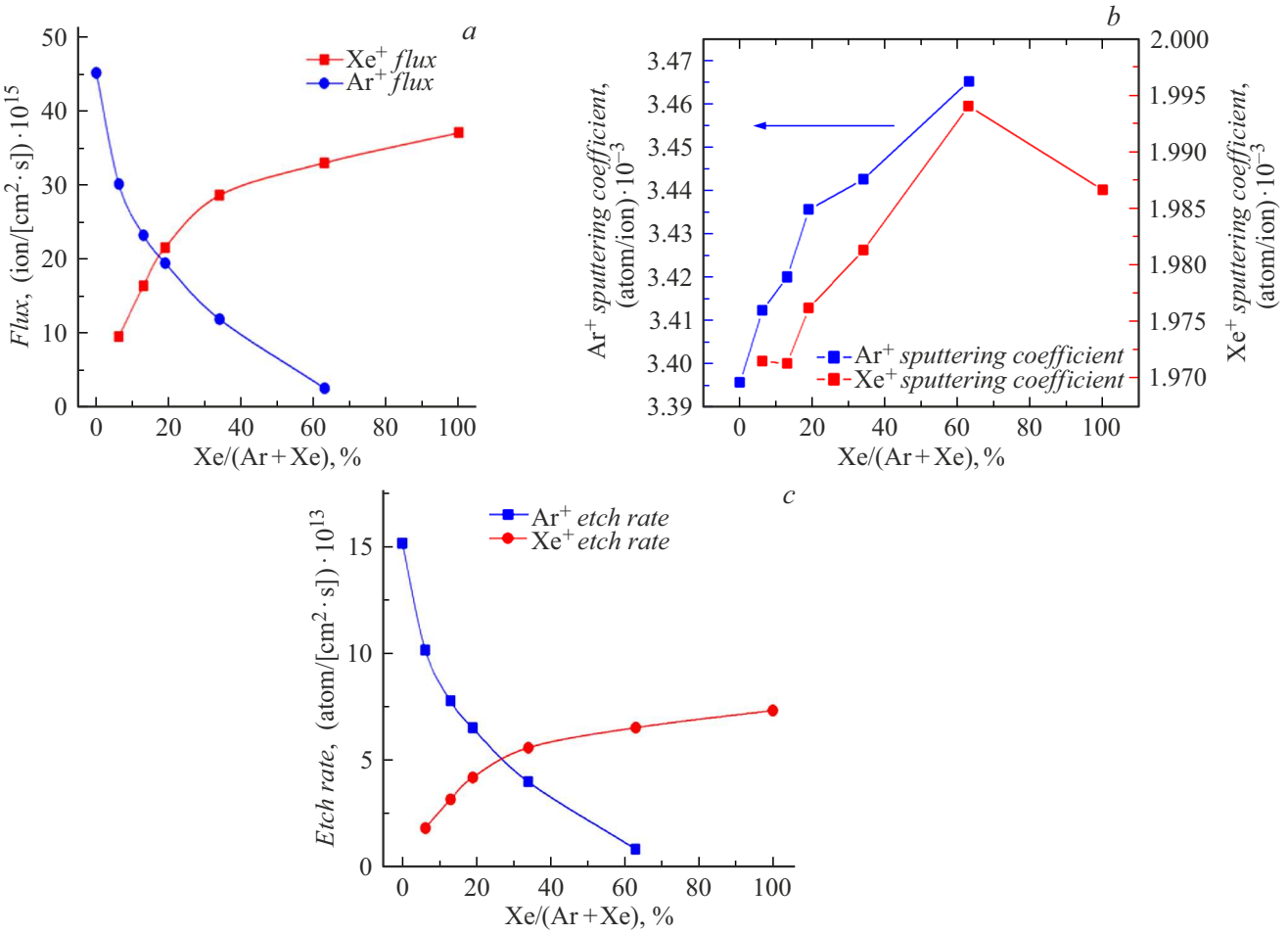

Figure 9. *a* — Dependence of the ion flux to the wafer surface; *b* — sputtering coefficient; *c* — simulated Ar^+ and Xe^+ sputtering rate as a function of the initial fraction of Xe in the plasma-forming mixture.

• An increasing amplitude of bias voltage V_{rf} induces a linear increase in average energy of ions E_{av} and makes the distribution wider (increases ΔE) due to an enhancement of electric field strength in the plasma sheath. The role of frequency ν_{rf} is to narrow the IEDF down by averaging the energy over the oscillation period, which is crucial for minimizing the energy spread in ALE processes.

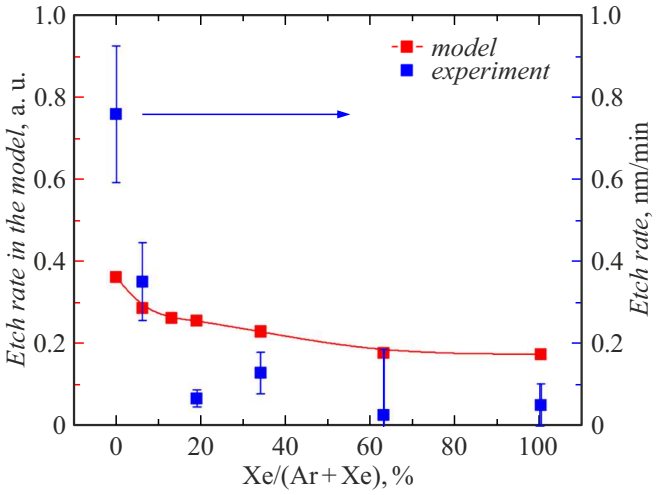

Figure 10. Sputtering rate as a function of the initial fraction of Xe in the plasma-forming mixture. The experiment was conducted at $p = 10$ mTorr, $W_{icp} = 1500$ W, and $V_{dc} \sim 30$ V.

• With the W_{icp} power increasing to 2500 W, electron temperature T_e increases by 25 % and plasma density n_e grows, leading to broadening of the IEDF due to shortening of the Debye length. At pressures > 10 mTorr, the transition to the collisional mode reduces E_{av} by 25 %.

• Added Xe (> 15 %) expands the IEDF for Ar^+, but the effect is less pronounced than that for Xe^+, since heavier ions have a longer transit time through plasma sheath. The gas mixture composition also has a profound influence on the dynamics of ion fluxes, suppressing strongly the flux of Ar^+ with the addition of Xe < 60 % due to the suppression of Ar ionization in favor of Xe. As the percentage of xenon in the plasma-forming mixture grows further, Xe becomes dominant in both ionization and sputtering processes. The composition of the gas mixture also affects the sputtering rate. The maximum sputtering rate of silicon in the experiment was achieved for pure Ar (≈ 0.9 nm/min), but

this entails a risk of damage due to a wide IEDF. According to the simulated data, the addition of Xe > 20 % reduces the overall sputtering rate by 40 %, which may be used to enhance the synergy in ALE due to a narrow IEDF.

The model presented above allows one to obtain IEDFs based on the results of plasma simulations, the input data of probe diagnostics at various plasma setups, and in various multicomponent gas mixtures, providing both energy spectrum optimization for ALE and sealing of porous low-k-dielectrics by a combination of low- and high-energy ions.

Funding

This study was carried out under the state assignment of the National Research Center „Kurchatov Institute“.

Conflict of interest

The authors declare that they have no conflict of interest.

References

[1] M. Bogdanova, D. Lopaev, T. Rakhimova, D. Voloshin, A. Zotovich, S. Zyryanov. Plasma Sourc. Sci. Technol., **30**, 075020 (2021). DOI: 10.1088/1361-6595/abf71b
[2] A. Fisher, Th. Lill. Phys. Plasma, **30**, 080601 (2023). DOI: 10.1063/5.0158785
[3] E.N. Voronina, A.A. Sycheva, D.V. Lopaev, T.V. Rakhimova, A.T. Rakhimov, O.V. Proshina, D.G. Voloshin, S.M. Zyryanov, A.I. Zotovich, Yu.A. Mankelevich. Plasma Proc. Polymer, **17** (2), 1900165 (2020). DOI: 10.1002/ppap.201900165
[4] A.A. Sycheva, E.N. Voronina, T.V. Rakhimova, L.S. Novikov, A.T. Rakhimov. J. Vac. Sci. Technol., **38**, 053004 (2020). DOI: 10.1116/6.0000389
[5] S. Robertson, Z. Sternovsky. J. Phys. Rev. E, **67** (2003). DOI: 10.1103/PhysRevE.67.046405
[6] T.V. Rakhimova, O.V. Braginsky, V.V. Ivanov, T.K. Kim, J.T. Kong, A.S. Kovalev. IEEE Transactions Plasma Sci., **34** (3), 867 (2006). DOI: 10.1109/TPS.2006.875849
[7] E.V. Shun'ko. *Langmuir probe in theory and practice* (Universal Publishers, Boca Raton, 2008), 245 p.
[8] F.F. Chen. Plasma Sourc. Sci. Technol., **18**, 035012 (2009). DOI: 10.1088/0963-0252/18/3/035012
[9] V. Kuzmenko, Y. Lebedinskij, A. Miakonkikh, K. Rudenko. Vacuum, **207**, 111585 (2023). DOI: 10.1016/j.vacuum.2022.111585
[10] V.O. Kuzmenko, A.V. Myakonkikh, R.R. Khalilullin. *Modelirovanie funktsii raspredeleniya ionov po energiyam v protsessakh plazmennogo travleniya.* In *Perspektivnye materialy i tekhnologii (PMT-2024)* (MIREA - Ross. Tekhnol. Univ., M., 2024), pp. 352–356 (in Russian).
[11] COMSOL 5.4. Plasma Module User Guide, COMSOL corp., 2018.
[12] A.V. Phelps. J. Physics B: Atomic, Molecular Opt. Phys., **33** (16), 2965 (2000). DOI: 10.1088/0953-4075/33/16/303
[13] V. Puech, S. Mizzi. J. Phys. D: Appl. Phys., **24** (11), 1974 (1974). DOI: 10.1088/0022-3727/24/11/011
[14] A.I. Saifutdinov. Plasma Sourc. Sci. Technol., **31** (9), 094008 (2022). DOI: 10.1088/1361-6595/ac89a7
[15] C. Lee, M.A. Lieberman. J. Vac. Sci. Technol. A, **13**, 368 (1995).
[16] G.M. Grigorian, N.A. Dyatko, I.V. Kochetov. Plasma Phys. Rep., **41**, 434 (2015). DOI: 10.1134/S1063780X15050049
[17] A.I. Saifutdinov, A.A. Saifutdinova, B.A. Timerkaev. Plasma Phys. Rep., **44** (3), 359 (2018). DOI: 10.1134/S1063780X18030066
[18] A.N. Kropotkin, D.G. Voloshina. Phys. Plasma, 053507 (2020). DOI: 10.1063/5.0003735
[19] Yu.P. Raizer. *Fizika gazovogo razryada* (Nauka, M., 1992) (in Russian).
[20] D.R. Shibanov, D.V. Lopaev, S.M. Zyryanov, A.I. Zotovich, K.I. Maslakov, A.T. Rakhimov. J. Appl. Phys., 134 (2023). DOI: 10.1063/5.0160531
[21] *The Plasma Data Exchange Project* (LXCat URL: https://nl.lxcat.net/home/ (date of access: February 08, 2025))
[22] T.V. Rakhimova, O.V. Braginsky V.V. Ivanov, A.S. Kovalev, D.V. Lopaev, Yu.A. Mankelevich. IEEE Transactions on Plasma Sci., **35** (5), 1229 (2007). DOI: 10.1109/TPS.2007.905201
[23] C. Bundesmann, H. Neumann. J. Appl. Phys., **124** (23), 231102 (2028). DOI: 10.1063/1.5054046

Translated by D.Safin